Macromolecules
ARTICLE

Macromolecules **2010**, *43*, 2421–2429 **2421**
DOI: 10.1021/ma902363p

Unrevealed Self-Assembly and Crystallization Structures of Na−Alginate, Induced by the Drying Dynamics of Wetting Films of the Aqueous Polymer Solution

H. Haidara,* L. Vonna, and L. Vidal

Institut de Science des Matériaux de Mulhouse (IS2M), LRC 7228-CNRS/UHA 15, rue Jean Starcky B.P. 2488, 68057 Mulhouse Cedex, France

Received October 23, 2009; Revised Manuscript Received January 29, 2010

ABSTRACT: Sodium alginate is a natural, water-soluble polysaccharide polymer which is not known so far to crystallize spontaneously. Here we show that the controlled drying of wetting films of the aqueous solution of this biopolymer can lead to the formation of large-scale self-assembly and crystallization structures. We show that the structures which grow exclusively within the final drying spot arise from the ordered assembly of the concentrated polysaccharide chains mediated by the condensation of trace cations present in the system. Moreover, we show that these trace cations, which are dragged with the polysaccharide chains and concentrated by the drying process inside the residual spot, come mainly from the ultrapure water used for the experiment. This study does not bring only new insights on the behavior and structural properties of polysaccharide polymers. It also shows that the use of water, even of high purity (conductivity $\leq 1\ \mu S \cdot cm^{-1}$), can lead to singular and unexpected effects when dealing with sensitive materials and experiments (polysaccharide/DNA, drying drops).

1. Introduction

In a series of papers[1−3] that was recently dedicated to wetting-induced morphological reconstructions of alginate-based coatings, it was shown that some of these reconstructions could drastically modify the initial morphology and the related functional properties of the coatings. Depending on the nature (pure alginate, alginate-based formulations) and drying morphology of the coating, these reconstructions can take place during the spreading of the deposited drop or appear in the wet spot after the drop has dried.[2,3]

In this paper, we deal with one of these wetting-induced structures, which here occurs on sodium−alginate coatings during the drying of wetting films of the aqueous polymer solution on silicon or glass substrates. Indeed, we show that the drying of wetting films of pure Na−alginate solutions prepared using ultrapure water can produce, under well-defined conditions, crystallization structures that appear inside the final drying spot at the end of the evaporation. These final drying spots and crystallization patterns, of which a general view is shown in Figure 1, are composed of an assembly of well-defined *dendrites* crystals. Compared to most reported wetting-induced patterns in polymer coatings,[1,4,5] the self-assembly structures appearing here originate directly from molecular-scale interactions between randomly distributed chains, leading to unrevealed crystallization patterns in a polymer, which usually forms crystalline phases only under strong and oriented stress fields.[6,7] Indeed, alginate is a polysaccharide whose chains consist of regularly alternating blocks of L-guluronic acid $(G)_n$, D-mannuronic acid $(M)_m$, and $(MG)_p$ residues (Figure 2) which have strong conformational differences.[6−8] This conformational mismatch which hinders the lateral ordering and packing between G, M, and MG residues also impedes any long-range structural organization and packing order (self-assembly) of these polysaccharide chains, and in particular, their *spontaneous* crystallization. Indeed, we did not find any reference or mention of the existence of a crystalline phase of sodium alginate in the numerous works devoted to phase diagrams of this biopolymer, either as a function of the alginate/water concentration, the pH, the ionic strength, etc.[9−11] Where crystalline or highly ordered alginate phases have been described, these have been exclusively produced by shear-induced orientation of fibers or thin films.[6−8] In this regard, the self-assembly and crystallization structures of alginate, which we show here that they form during the drying of wetting films of Na−alginate solutions, in relatively mild conditions (evaporation-drying dynamics), represent both a new and unexpected result. And as such, these results can contribute to a deeper understanding of the structural properties of this widely used and still promising biopolymer, for applications covering nanotechnologies and bioengineering.[12,13] For instance, alginate and other polysaccharide polymers are used as functional coatings in inkjet printing of textile fabrics to control the impregnation of ink droplets and the diffusion of dyes in the fabrics.[14,15] In these applications, for instance, wetting-induced morphological reconstructions like the crystallization structure reported here can occur on the coating, affecting thereby its functional properties and efficacy.

In the following, we first present the Experimental Section describing the materials, the preparation of the samples, and the methods. Then, we consider in a dedicated section the different possible hypotheses which can explain the formation of the crystallization patterns. The discussion of these hypotheses, each of which was checked experimentally has naturally led us to the most plausible mechanism, i.e., the crystallization of alginate after the condensation of a critical amount of Na^+ cations on the polyanions chains. The discussion of this mechanism on the basis of reference works on the structural behaviors of polysaccharide polymers in general, and of Na−alginate in particular, constitutes the corpus of the paper in next sections.

*Corresponding author. E-mail: hamidou.haidara@uha.fr.

Published on Web 02/12/2010

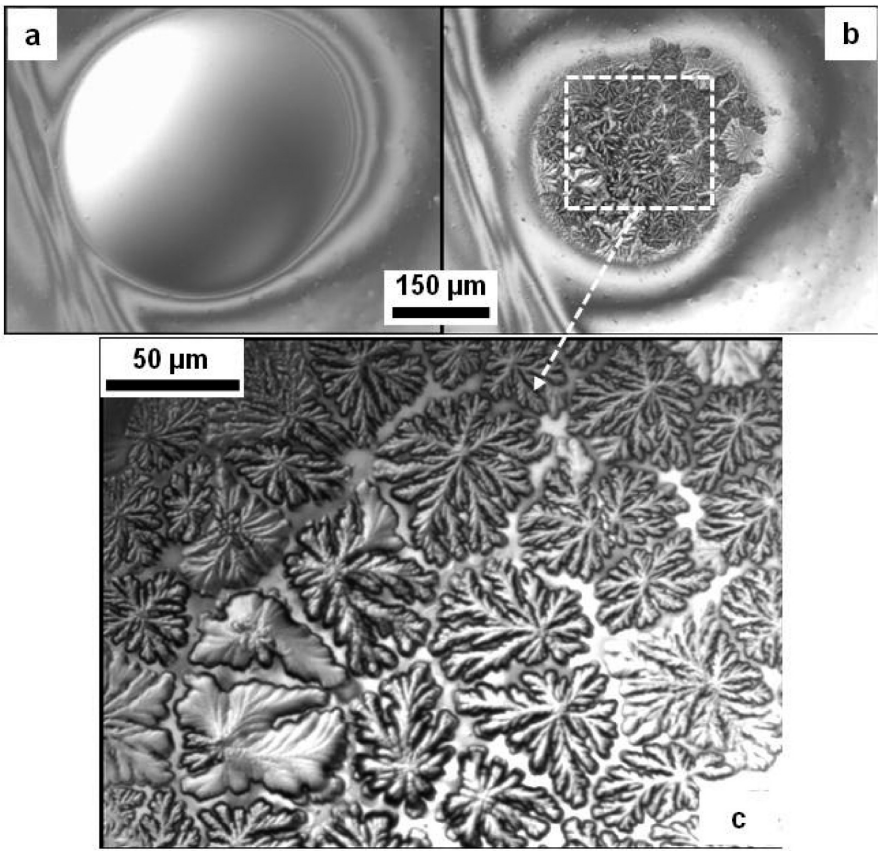

Figure 1. Drying mediated crystallization structures of sodium−alginate (SA) produced by a wetting film of SA solution. The results shown here were obtained by the evaporation-drying of 50 μL of centrifuged SA solution of concentration, $C = 0.125$ wt % (12 μmol/L), on a square silicon plate of 2.5 cm^2. Key: (a) residual droplet, right before structure formation time $t = 0$, (b) ~50 s after the structure formation has started, and (c) close view of dendrites crystals that form in the final dry spot at $t \rightarrow \infty$.

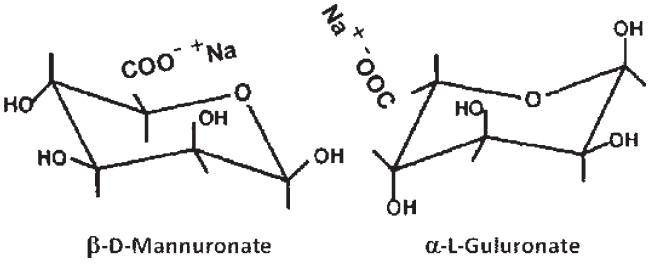

Figure 2. Chair structure of the Mannuronic and Guluronic acid units constitutive of Na-Alginate chains.

2. Experimental Section

2.1. Materials and Sample Preparation. Alginic acid sodium salt from brown algae hereafter referred to as sodium alginate (SA) was purchased from Sigma-Aldrich. It is described as a medium viscosity polyuronic acid (viscosity ≥2 Pa·s at 2 wt % in water), composed primarily of anhydro-β-D-mannuronic acid residues with 1 → 4 linkage. The average molecular weight of this alginate was given by Aldrich to range in between 80000 and 120 000 g/mol (average $M_w \sim 100\,000$). Aqueous stock solutions of 2.5 wt % SA were prepared by dissolving the alginate powder into warm water (60 °C) under strong mechanical stirring for 30 min. This stock solution corresponds in average to the alginate concentration generally used in the literature[16] and for functional applications as thickener coatings.[1−3] Lower alginate concentrations of 0.25 and 0.125 wt % were prepared from this stock solution. Reverse osmosis (Milli-Q) water of measured conductivity of 1 μS/cm was used for all experiments. In equivalent sodium chloride (NaCl) concentration, this conductivity corresponds to ~10^{-5} mol/L. The fresh solution which has a shear viscosity of ~3.5 Pa·s at 1 s^{-1} was cooled to ambient temperature and kept at ~4 °C, before and during use (1 week for each solution). (100) oriented single side polished silicon wafers which were cut into square pieces of two sizes (2.5 ± 0.2 and 1.3 ± 0.1 cm^2) were used as substrates. These pieces were treated for 30 min in warm (50 °C) piranha solution (mixture of 3 vol. of 30% H_2O_2 and 7 vol. of H_2SO_4), and thoroughly rinsed with pure water to create a clean, hydroxyl-rich surface. The substrates were then dried under ultra pure nitrogen flux before applying the alginate. This was done by forming a wetting film of SA by the spontaneous spreading of a solution drop.

2.2. Experimental Protocol. Basically, the experiment has consisted in depositing a drop of the SA solution, which is allowed to spread out in a wetting film covering the entire surface area of the substrate. After a certain time, this wetting film then starts to retract, driven by evaporation. The nominal thickness of the film was determined by the size of the substrate (2.5 ± 0.2 and 1.3 ± 0.1 cm^2) and the deposited volume of solution (25, 50, and 100 μL). A systematic study involving the SA concentration in the wetting film, the surface area initially covered by the wetting film and the corresponding volume of the deposited solution, has then been carried out to determine the influence of these parameters on the formation of the structures. The evaporation−retraction step, as well as the structural evolution of final drying spot are followed and recorded using a video-microscope (Olympus optical microscope), equipped with DIC (differential interference contrast) device, and a COHU solid state CCD camera operating at 24 images/s. All the experiments (deposition of the drop, spreading and formation of the wetting film, evaporation, retraction to complete drying) were performed under the ambient conditions of 22 °C and 35% RH.

Before arriving at the final results of this work to be presented and discussed in the last section, we present first, in what

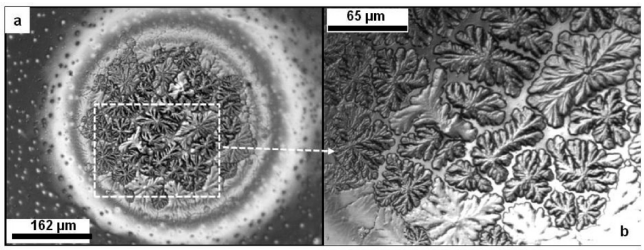

Figure 3. Drying of a wetting film of 50 μL of *raw* SA solution of concentration, $C = 0.125$ wt % (12 μmol/L), on a 2.5 cm^2 substrate. Key: (a) the insoluble particles, which are present in the raw solution and visible around the residual spot do not affect the formation of the structures; (b) not only the structures are formed, but they are as well-defined as with *centrifuged* SA solutions, once the required conditions are satisfied (drying induced confinement and packing, concentration of polysaccharide and Na^+).

follows, the different hypotheses (more or less plausible) that could account for the formation of the observed structures.

3. Possible Hypotheses on the Formation of the Crystallization Pattern

There are three main hypotheses which can be retained within this experiment as potentially capable to induce the formation of the observed wetting and drying structures in the alginate coating. These are (1) the aggregation of dust or insoluble particles either contained in water or in SA itself, (2) the crystallization of residual salt that might be contained in water or in the coating, especially Na and Cl ions involved in the two main synthesis routes of SA from brown algae, and (3) the self-assembly and crystallization of SA chains mediated by the condensation of the residual Na^+ cations, and assisted by the wetting dynamics. This later hypothesis is hereafter referred to as, "residual Na^+ mediated SA crystallization".

3.1. The possible role of dust or contaminants which may exist on the bare Si substrate or in water has been checked by the evaporation-drying of pure water drops on Si substrate. The evaporation and retraction of these drops toward the complete drying were followed under the same conditions as for the drying SA wetting films. In the rare cases where particle aggregates were visible in this check experiment, these were composed only of a few isolated and featureless dust clusters. Obviously, the crystallization structures that form with SA wetting films (Figure 1, and Figure 3) have nothing to do with these discrete dust clusters, neither in their structure and organization, nor in their composition as attested by complementary scanning electron microscopy observation and analyses (Supporting Information, part 1).

Regarding the insoluble particles that may exist in SA, we showed that experiments either performed using solutions centrifuged at 15000 rpm for 40 min, or using the "raw" solutions systematically lead to identical results (formation or absence of structures), under identical conditions. This is well illustrated in Figure 3 where fine self-assembly and crystallization structures similar to those shown in Figure 1 are formed in wetting films of raw (noncentrifuged) SA solutions containing insoluble particles that are visible around the final dry spot. It is therefore clear from these results that the observed structures are not made of these insoluble particles, which, in addition were only partially dragged by the withdrawing front in the best case. On the other hand, these results do not completely exclude the possible presence of crystallizable molecular/atomic-scale trace contaminants originally contained in SA, which can be fractionated by the receding front and concentrated in the final dry spot. In the following, we show on the basis of our results that this hypothesis is simply very improbable.

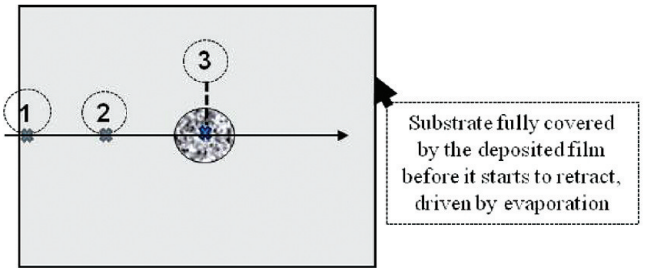

Figure 4. EDX compositional analysis of a structure forming sample. Zone 1: reference virgin SA coating corresponding to shortest dwell time with water. The average atomic composition of this zone in atomic % is C = 42 ± 2, O = 51 ± 1, Na = 5, and Cl ≡ 0, giving ratios of (Na/C) = 0.12 and (O/C) = 1.21, including C and O contributions from possible organic and Na_2CO_3 trace contaminations, as well as O from SiO_2 (substrate). Zone 2: SA coating with longer dwell time in water; the average atomic composition of this zone is C = 41 ± 1, O = 51.5 ± 0.5, Na = 4.8 ± 0.2, and Cl = 0.1 ± 0.1, giving ratios of (O/C) = 1.24, (Na/C) = 0.12, (Cl/C) = 0.002, and (Cl/Na) = 0.02. Zone 3: final dry spot (crystals) where SA chains have experienced the longest dwell time with water; the average atomic composition in this zone is, C = 43 ± 2; O = 38 ± 2, Na = 12.8 ± 0.4, and Cl = 6.5 ± 1, giving ratios of (O/C) = 0.88, (Na/C) = 0.3, (Cl/C) = 0.15, and (Cl/Na) = 0.5.

3.2. To check the hypothesis of a possible role, and of a crystallization exclusive of the residual salt contained in SA solution, we have undertaken to quantify, by a systematic elemental analysis, the salt traces and their spacial distribution on the dried coating, on which the structures appear. The analyses were performed in an environmental scanning electron microscope (FEI, model Quanta 400), using an EDX (energy dispersive X-ray) spectroscopy module for elemental analysis. The EDX spectra (Figure 4) were taken along the dry SA film, from the outer region, toward the final dry spot where the structures form. The main results of these EDX analyses are summarized below schematically in Figure 4 (Supporting Information, part 2). The first information provided by these spectra is that sodium is the only salt ion which is found in the outermost region of the sample that dries first, and thus constitutes the part of the SA film which remains confined for the shortest time with the solvent (water) and the possible "contaminants" it could contain. No chlorine (Cl) or calcium (Ca) were found at a level detectable by EDX in this outermost region of "virgin" coating whose spectrum reveals exclusively C, O, and Na, i.e., elements that are constitutive of SA polymer (Figure 2). As a result, one can reasonably attribute the Na found in the virgin region of the coating to those bonded originally to the carboxylates of the Na−alginate chains during the synthesis of SA from alginic acid. The second information provided by these analyses is that the concentration of both Na and Cl increases from the border of the deposited film, first as traces for Cl, to reach a maximum inside the final drying spot. This definitely shows that the occurrence of the salt elements in the film, i.e., Cl, and Na in excess of those originally bonded to SA chains is exclusively related to the water solvent, with the concentration of Na and Cl increasing with the dwell time of the coating in water (increasing evaporation time toward the final dry spot). It is worth noting and stressing here that what really matters regarding the interaction and conformation of the SA chains is the available free Na^+ cations, which condense on the chains and control their conformational organization, irrespective of their origin (NaCl or Na_2CO_3). Therefore, some of these Na^+ cations may come from Na_2CO_3 initially contained in

water as trace contaminants, although EDX could not specifically detect C and O atoms issued from the CO_3^{2-} counterpart of Na_2CO_3, contrary to Cl counterpart of NaCl. Therefore, we here focus in the following on NaCl, not only as a potential contaminant of water (although not the most likely) but also as a simple salt compound which can be used as a source of free Na cations in the experimental modeling of the crystallization process. Finally, regarding the hypothesis of crystallization structures which are exclusive of residual salts, we prepared a solution of salt of concentration equals to that determined in average inside the final dry spot, right on the structures. This was done by assuming the salt to be composed essentially of NaCl, the amount of which is determined by that of the lowest concentration constituent (Cl here), since Na atoms which preexist in SA carboxylates counterions are in excess to those introduced by salt traces issued from water. Thus, assuming the crystallization spot to be essentially made of the "SA/salt" compound (wt % of C, O, Na, and Cl), and taking an equal amount of Cl and Na in *atomic* %, a concentration of NaCl inside the dry spot was estimated, and found to be equal to ~20 wt %.[17] We tested this salt concentration with the high viscosity SA solution (2.5 wt %), keeping in mind that the 20 wt % salt refers to the mass of (polymer/salt) after complete drying, and not to the weight (mass) of the starting aqueous solution (water/polymer/salt). A priori, the drying of the wetting films of this solution should lead, upon drainage, to a NaCl concentration in the final spot, which is much higher than the one estimated above from EDX in the crystallization pattern. Furthermore, this solution should be so close to the crystallization conditions that the structures should develop much earlier after a small amount of water is evaporated. We did these experiments and have observed that crystallization actually appears very rapidly in this case, with structures which are much larger and finer (Figure 5a,b), while covering almost the whole wetting film (total area of the sample). Indeed, since the growth of the structures appears in this case typically at coverage of the wetting film which is about half-size of the initial one, the wetting film does not retract completely. On the other hand, when a drop of the "pure" aqueous solution of identical NaCl concentration is dried under similar conditions, no structure is observed, except a few isolated polyhedral crystals (Figure 5c,d). When compared to the drying structures produced above by the wetting film of the aqueous (SA/NaCl) solution, which almost entirely cover the whole film, this result shows at least that the polysaccharide well represents the preeminent constitutive element for the structure formation. Additional evidence toward this result is brought by the parametric studies presented and discussed in the next section "Results and Discussion".

In summary, it seems unlikely that one of the exogenous factors considered above (dust/contaminants, insoluble particles, or salt crystallization) played any role in the genesis of the structures which are observed here. On the other hand, while the drying of the salt solution at the concentration found in the crystallization pattern was not found to produce alone the structures, the check experiments show that a SA film with this salt concentration could "instantly" produce, on large scale, similar crystallization structures (Figure 5a,b). This leaves us with the only remaining and plausible hypothesis regarding the genesis of the structures, i.e., the ordered assembly of the polymer chains, mediated by the condensation of trace cations present in the water, both components being concentrated within the final dry spot by the evaporation-driven retraction dynamics. The phenomenological framework of the drying and related drag process which here drives the structure formation is briefly presented below.

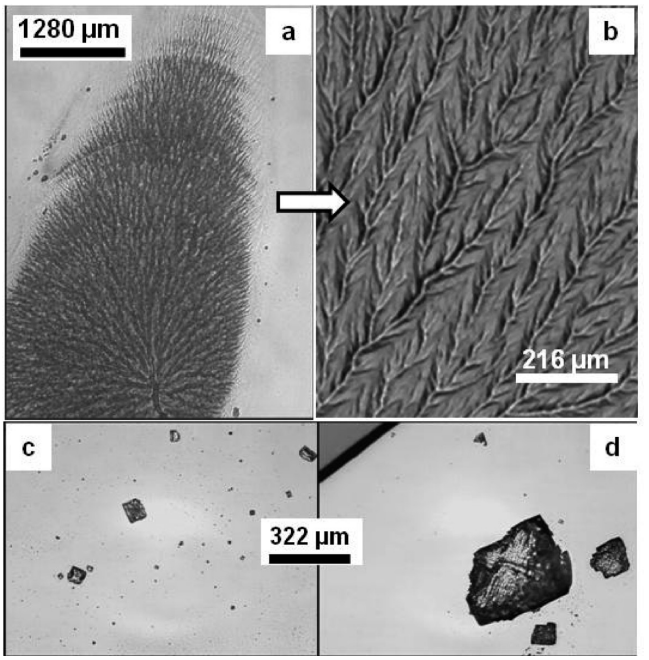

Figure 5. Check experiments on the role of the residual and added salt (NaCl) performed using 100 μL SA solution of concentration, C_{SA} = 2.5 wt % and C_{NaCl} = 0.5 wt %, on a 2.5 cm^2 substrate. Key: (a) drying spot and (b) a magnification of the arborescent structures formed in drying SA wetting films (note that the pattern shown in the drying spot (a) represents almost one "single" structure); (c, d) drying pattern produced by the same volume of pure NaCl solution of identical concentration (0.5 wt %). Obviously the few isolated "crystals" that form in this case have nothing to do with the patterns produced in presence of SA.

4. Phenomenological Framework of Wetting-Assisted Drainage and Structure Formation

Basically, the evaporation drying dynamics and related drainage events leading here to a concentration in the final drying spot which is much higher than the nominal (initial) one are essentially driven by the balance between two forces. These are on the one hand, the imbalanced capillary force which drives the motion of contact line and provides the drag exerted on particles in the wetting front, and on the other hand, the resistance to the drag which arises either from the adhesion, or the viscous friction.[18−20] For chains that are located at the substrate/fluid interface and loosely attached to the substrate, the dominant resisting force to the drag is the viscous shear. The capillary force is determined by the extent of the departure between the quasi-equilibrium contact angle θ_e achieved at the end of the spreading, and the dynamic contact angle of receding, θ_r. This departure gives with the surface tension γ_L of the fluid, the capillary force per unit length[19,20]

$$\mathbf{F}_c = \gamma_L(\cos\theta_r - \cos\theta_e) \quad (1)$$

In the limit of small but finite contact angles (typically $\theta < 1$ rad), this amounts to[19]

$$\mathbf{F}_c \sim \frac{1}{2}\gamma_L(\theta_e^2 - \theta_r^2) \quad (2)$$

The viscous force $\mathbf{F}_\eta$ (per unit length) is related to the viscosity of the film η_f and the velocity $\mathbf{v}$ of the receding front of the

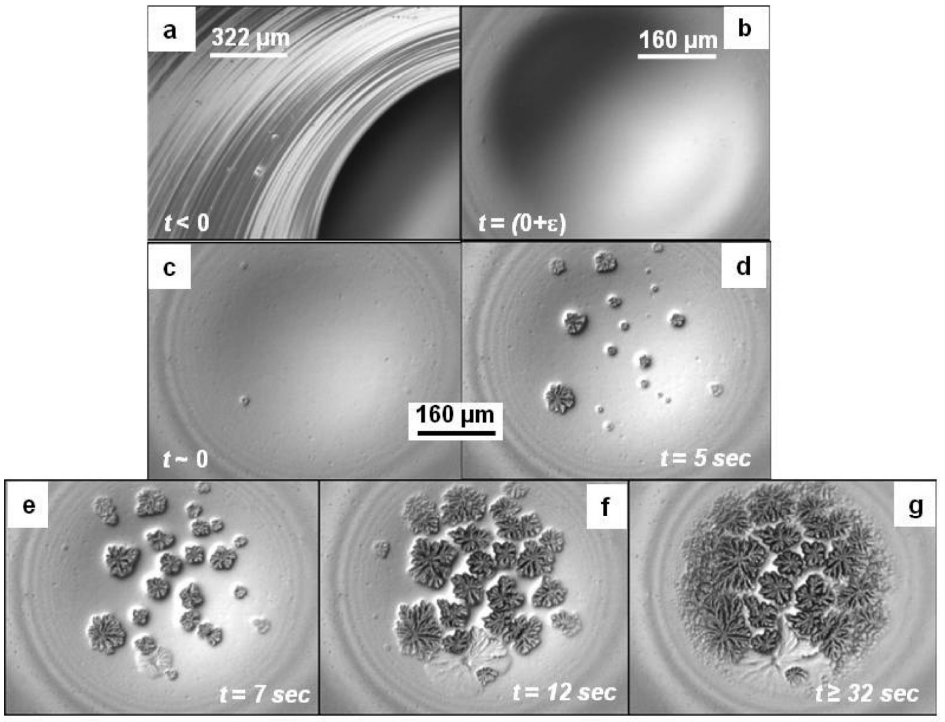

Figure 6. Kinetic sequence of the growth of the structures for a drying wetting film of 100 μL of centrifuged SA solution of nominal concentration $C = 0.25$ wt % (25 μmol/L), on a 2.5 cm^2 Si substrate. Key: (a) oscillations of the thickness of the deposited polymer induced by the stick−slip motion of the receding front of the evaporating film; (b) final drying spot containing the emerging crystallization pattern.

paddle wetting film, which collects the chains, and is given at first order by[19,20]

$$\mathbf{F}_\eta \sim 3\eta_f \mathbf{v} L/\theta_r \tag{3}$$

where $L \approx \ln[\theta_r^2(w/a)]$ is a logarithmic factor that accounts for the divergence of the dissipation in the wedge, through the ratio of the lateral size of the wedge (w) to a cutoff length (a), which is of molecular size. L is typically on the order of 10.[19]

For the three concentrations of SA used in this work, the values of the contact angles θ_e and θ_r of the solution, relative to its own thin, and highly viscous film adhering to the Si substrate (Supporting Information 3) are typically ~20° and ~5°, respectively, for a surface tension of the solution of ~66 mN/m. For the medium concentration of 0.25 wt % SA (0.25 g in 100 mL water), which has a viscosity η of ~0.2 Pa·s, one expects for evaporation-drying experiments involving wetting films of this solution to have a velocity of the receding front that scales as [eqs 2-3],

$$\mathbf{v} \approx \gamma_L(\theta_e^2 - \theta_r^2)\theta_r/12\eta L \tag{4}$$

This gives a velocity $\mathbf{v}$ of ~0.026 mm/s, which is of the order, but two times higher than what we determined on average from experiments (~10^{-2} mm/s). As well for experimental reasons as for the numerical values considered in the eq 4, we could naturally expect some discrepancy between the estimated speed, and that measured experimentally. Indeed, during the drying of the wetting film, the viscosity gradually increases, especially around the contact line of the retracting film. As a result, the value of the viscosity η_f which should be considered in eq 4 is not the nominal one of 0.2 Pa·s, but a time-dependent viscosity, the time-averaged value of which is probably much higher, especially at the end of the drying. In addition, due to the stick−slip events and the related thickness fluctuations already discussed above and visible below in Figure 6a, the receding velocity is not constant over the entire drying cycle (Supporting Information 4). These stick−slip events and related thickness fluctuations arise here from the time-variation of the evaporation rate at the wetting front. This phenomenon is essentially different from the usual Marangoni convective flow and the involved solutes transport, which results from an evaporation gradient along the drop (from center to edge), and which often leads to the well-known concentric particle rings, in drying suspension drops.[21] But at the difference of such suspensions where the solutes (particles) are free to move, transported by the convective current, the movement of the polysaccharide chains is here strongly impeded by the high viscosity of the solution (chains entanglements). The evaporation events (gradient along the drop and convective flow), which are in addition very low here because of the flatness of the wetting film are therefore essentially confined to the edge of the drying film. As a result, there is no depletion of the drop (volume) in polymer chains due to the convective migration to the edge. In other words, the drying dynamics, and the drag in particular, should further concentrate the polymer in the final spot, leading thereby to a concentration which is much higher than the nominal one. Finally, besides the thickness undulations, which we here attribute to local time-variations of the evaporation rate at the edge of the wetting, the above stick−slip events have no determining effect here on the structure formation. This would have been the case only if the stick was irreversible (complete pinning), in which case the film would have dried on an area that is much larger, leading to subcritical concentrations of polymer and cations for the structure formation. The above results and discussion essentially highlight one parameter, determined by the drying dynamics, which controls the observed structure formation. This is the drag and packing (concentration) of the solutes (chains and cations) within the final spot. The drying dynamics being strongly dependent on the experimental conditions, especially the nominal concentration of the polymer, the contact angle $\theta(\gamma_{substrate})$, the RH, or T°, it should be noted that changing any of these conditions can drastically impact this drying dynamics. These conditions thus provide some key parameters to tune the structure formation by either adjusting the receding velocity $\mathbf{v}$, the stick−slip versus complete pinning, and the extent of the final drying area.

Table 1. Dependence of the Structure Formation on the Total Amount of SA Chains in the Deposited SA Solutions, As Determined from the Drying of Two Wetting Films of Identical Volumes (25 μL) and Extent of Interface Area (1.3 cm^2 $\pm$ 0.1), but Significantly Different Nominal Concentrations (0.25 vs 0.125 wt %) in SA

	occurrence of structure		
	1st experiment	2nd experiment	3rd experiment
C_{SA} = 0.25 g/100 mL (2.5×10^{-5} mol L^{-1})	none	yes	yes
C_{SA} = 0.125 g/100 mL (1.25×10^{-5} mol L^{-1})	none	none	none

5. Further Results and Discussion

The sequence of top view snapshots shown in Figure 6 represents the intermediate and the very late stages of a typical evaporation−drying experiment. The first image (Figure 6a) is a micrometer-scale scale view of the wavy pattern induced in the deposited film by the stick−slip oscillations of the receding front as discussed above. The following snapshots are more closely related to the genesis of the crystallization pattern, highlighting the structural changes preceding and accompanying the growth sequence of the dendrites crystals inside the residual spot, in the final stage of the evaporation. Whenever the drying leads to crystallization patterns, the first changes that predict the emergence of the structures are (1) the gradual and strong increase in the viscosity of the solution which significantly reduces the withdrawal velocity (in agreement with eq 3) and (2) the appearance of a bump on the final wet spot (Figure 6b). Figure 6c shows the deflation of the bump which results from the drying and the volume relaxation due to the structural reorganization of the chains inside the spot. This deflation is followed by a roughening of the wet residual spot (which may be observed or not), before the "nucleation" of the first dendrite crystals. The nucleation starts randomly, either at the border or at the center of the spot, and propagates, both by growth and further nucleation (Figure 6d−g) to completely cover the residual spot. As seen from Figure 6g, there is no significant change in the morphology of the structures which will essentially go through a maturation involving their dehydration and the "complete" drying of the spot. Finally, this growth kinetics revealed that the spatial extension of early formed crystals is stopped, essentially because they meet other growing crystals (Supporting Information 5a,b). In other words, the material available in the residual spot might largely suffice to feed the growth of one single crystal, if we could favor the exclusive growth of the first appearing crystal. Whether the appearing structures form in the residual solution (and therefore preexist), and emerged only on complete drying, as already shown for the formation of wormlike aggregates in drying drops of nanocolloid suspensions,[22] or are nucleated from the substrate during the final drying, remains an open-question. In both cases, a critical concentration of the solutes (polymer and cations here) is required for the crystallization to develop, as already known for the evaporation-induced crystallization of polymer and minerals.[23,24] However, at the difference of those highly soluble species that readily crystallize above a critical concentration under controlled evaporation conditions, SA polysaccharide remains a poorly water-soluble polymer, which forms highly viscous sol (or gel) at quite low concentration (< 5%). In these polysaccharide solutions where the solvent is sequestered within the interpenetrated chains network at high concentration (high viscosity), never has a bulk crystallization been reported, regardless of the way the evaporation is conducted (high or low rate). The other way around to observe such bulk crystallization would be the direct dissolution of SA up to the critical (saturation) concentration. But practically, this is hardly achievable under soft conditions, the preparation of such high bulk concentration (close to saturation), requiring the dissolution of SA in water under mechanical stirring as usual. Indeed, the solution to be prepared in this case should have a concentration close to that existing in the tiny volume ($\sim 10^{-4}$ μL) of the final bumps (Figure 1a and Figure 6b) preceding the emergence of the crystals. Considering the size, the density and extent of the structures inside the spot, one can assume this critical concentration of polysaccharide chains to be at least ~30 wt %, the remaining being water and concentrated salt traces. And as we noted above, this concentration or even much lower ones (15 or 20 wt %) are never prepared or achieved,[25−27] because such concentration (and viscosity) would require a mechanical stirring energy that definitely compromises any crystallization process. Most importantly, such bulk dissolution conditions do not create the geometrical confinement required for the structure formation, and ensured by the evaporation-drying dynamics inside the tiny final micrometersize spot. Besides the description of the growth sequence and features of the crystallization patterns, the basic question that thus remains unanswered here is the following: "By which mechanisms SA polysaccharide chains that are not known to spontaneously form crystals or highly ordered structures, can produce as well organized crystallization patterns under such smooth conditions?" We here propose a tentative mechanism, based on the most plausible conclusion of our check experiments and last parametric studies, i.e., the confinement of the concentrated polysaccharide chains, and their crystallization mediated by the condensation of Na^+ cations in the tiny residual spot. Indeed, in this last experiment, a smaller but identical volume (25 μL) of SA solutions of nominal concentrations, 0.25 and 0.125 wt %, were deposited on small size substrates of precisely identical surface area (1.3 cm^2 $\pm$ 0.1). In this case, we ensure that the amount of SA chains in the wetting film which fully covers the total surface area is lower, for the low concentration solution (0.125 wt %), whereas the amount of water and residual salt that it contains are higher, compared to the solution of higher concentration (0.25 wt %). In other words, the relative fractions (amounts) of polymer and water in these two solutions, an equal volume of which is spread out on the same surface area, are expected to lie in the following order,

$$[(\text{water} + \text{residual salt})/\text{SA chains}]_{0.125\%} > [(\text{water} + \text{residual salt})/\text{SA chains}]_{0.25\%} \quad (5)$$

Assuming now an increase of the cations concentration in the tiny residual spot to be *the preeminent factor* of the structure formation, we naturally expect that to happen for the low SA concentration, C = 0.125 wt % (1.25×10^{-5} mol L^{-1}), of higher amount in salt traces, and less probably for C = 0.25 wt % (2.5×10^{-5} mol L^{-1}). Our results summarized in Table 1 (and in Supporting Information 6 for corresponding structures) show that it is the opposite which actually happens. Although the size of the pattern was smaller compared to larger volumes of solution as one could expect, the occurrence of the structures for C = 0.25 wt % (25 μmol/L) was found to be *2/3* in average, versus *none* for C = 0.125 wt % (12 μmol/L). It is worth noting here that at the difference of the corpus experiments where SA solutions of higher volumes and concentrations were used, and where structures readily appear, the parameters of this last experiment (low volume and concentrations) were purposely adjusted to bring us close to the boundary between "structure formation" and "non-structure formation". Therefore, the non systematic occurrence of the structures in these last experiments was

expected, even for the 0.25 wt % solution (Table 1). Naturally, these results, and particularly the nonsystematic occurrence of the structures do not have any inference with the corpus experiments presented and discussed above, which were performed with SA solutions of higher volumes and concentrations (0.25 wt %, 100 and 50 μL).

First, this result shows that a threshold concentration of polysaccharide chains is required so that the crystallization, mediated Na^+ cations, can take place inside the final drying spot. This threshold concentration may be achieved for different starting nominal concentrations, depending on the conditions of the experiment, like the retention (deposition) of the polymer on the substrate during the evaporation−drying and retraction process. Second, and most importantly, this result definitely shows that polysaccharide chains (their concentration and confinement) are the preeminent constitutive element which determines critically the emergence of the crystallization structures. At the scale of the chains, the mechanisms that here drive the cations-mediated crystallization of the SA chains may be the same as the well investigated structural and conformational changes that drive the phase transitions in polyelectrolytes, and in particular, in SA polysaccharides.[25−28] These mechanisms involve first the screening of the anions (carboxylates) along the SA chains by the condensing Na^+ cations, as their concentration increases, reducing both inter- and intrachain repulsion (decrease of Debye screening length). An important consequence of this screening effect is that the persistence length of the chains, which is composed of an intrinsic part due to backbone rigidity L_b (bare persistence length), and of an electrostatic contribution L_e due to polyions charges will decrease, mainly through the term $L_e \sim (L_B C_S)^{-1}$,[25,27] which scales as C_S^{-1}, C_S being the salt concentration, and L_B the Bjerrum length.[25,27] There should therefore exist in terms of stoichiometry (ratio of counterions to chain anions), a concentration of monovalent cations (Na^+) for which a complete canceling out of the charges along the chains appears (complete screening). This means for our system that a concentration of Na^+ cations that condense and fully compensate the initially unbounded (free) carboxylates of the SA chains be reached in the final spot. As a result of that complete charge screening and increased flexibility, the chains can come into much closer contact, driven in that by the predominating van der Waals (vdW) forces, assuming the total interaction potential to be dominated by the balance between electrostatic repulsion, and vdW attractive forces (classical DLVO potential).[29] If the above requirements are combined with a high concentration of chains and Na^+ cations, as it is the case in the final tiny spot (confinement), a very short-range assembling (close packing) and organization of the chains, which is favored by their increased flexibility, can take place. These tentative interpretations of course remain essentially phenomenological at this step, because the observed phenomenon is quite new and quite unexpected. However, the mechanisms which we here propose for the formation of the self-assembly and crystallization structures were strongly comforted by an additional experiment which was suggested by a reviewer, and which we performed during the revision period of the Ms. The bottom idea here is the following. If one assumes relevant the hypothesis of conformation changes induced by Na cations, then the same effect can be induced by an acidic SA solution, leading to drying patterns similar to those produced by added salt (Figure 5a,b). Interestingly, the experiments that we did, using SA solutions at pH = 2, and keeping identical the conditions under which the structures occur with bare SA wetting films, have all lead systematically to the formation of crystallization patterns. Furthermore, not only the structures that form (crystallization spot and crystal size) are larger than those observed with "bare" SA solution, but they also appear under conditions (drying, concentration and substrate size) where bare SA solutions do not systematically lead to structure formation. In other words, experiments at acidic pH clearly improve (by enlarging) the conditions under which the crystallization structures appear. And most importantly, the structures that form at acidic pH are of comparable size (the overall crystallization domain), and have the same morphology as those produced by salt addition (Figure 5a,b). Because H_3O^+ ions adsorb and structure along the SA chains (polyanions) in a way similar to Na^+, one expects this process to lead at high pH to similar changes in chains interaction (dominant vdW and hydration forces) and conformation (decreased persistence length), and ultimately, to close contact, assembly and packing of the more flexible chains. These results thus support well our work hypothesis relying on such mechanisms. Finally, although this study was essentially focused on SA polymer, we have showed that the wetting-induced crystallization process that was observed and discussed in this work was not specific to this polysaccharide polymer. Indeed, we showed that the same evaporation-drying dynamics could induce the formation of similar crystallization patterns in wetting films of the "bare" aqueous solution of guar gum (Figure 7), an amorphous polysaccharide polymer which has much similar functional properties to SA (thickening, gelling, etc.). Although guar gum is a nonionic polysaccharide which bears exclusively hydroxyls groups, contrary to the carboxylate-bearing anionic SA, the genesis and the general features of the crystallization structures for the two polymers are similar, and may be accounted for by the same mechanisms, in the sense of the changes in chain conformation. Indeed, the conformational changes, from extended to flexible and collapsed chains, have been extensively studied for guar gum, and shown to be equally strongly affected by salts, depending on their nature and concentration.[30,31] More specifically, these works show that the influence of salt, when this exists, relies on the entropic ordering (salting-in), or disruption (salting-out) that they induce in the structure of water molecules surrounding guar gum chains, leading thereafter to a chain solubility, which is increased (extended chains), or reduced (more collapsed, formation of small length scale aggregates).[30,31] Interestingly, although this structuring effect was shown to be less pronounced for NaCl, it is on the other hand found to be very strong for Na_2CO_3, a rather common salt contaminant of water, which contributes to the overall Na^+ cations as we mentioned above. On the basis of this last result, it seems that the formation of these crystallization patterns in polysaccharides is a rather general phenomenon, which is underpinned by the same physics, as all our results show it: counterions condensation, ions-induced salt-out, confinement, shortening of Debye screening length, decrease of persistence length ~ increased flexibility, and chains packing. In this respect,

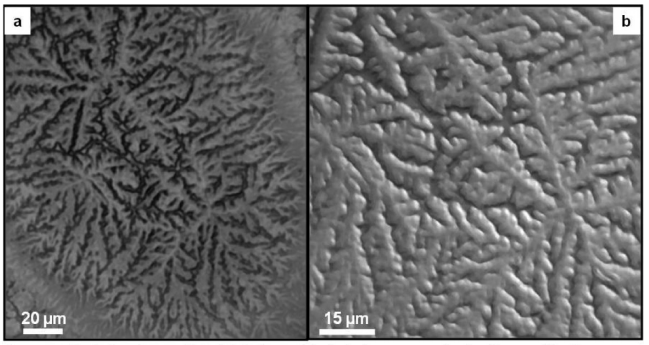

Figure 7. Optical micrographs of (a) the residual drying spot and related crystallization pattern generated by a wetting film of a *guar gum* solution of nominal concentration C = 0.25 wt %, on a 2.5 cm^2 Si substrate and (b) magnification showing some of the dendrite structures at the center of the crystallization spot. The guar gum (ref G4129) was from Sigma-Aldrich.

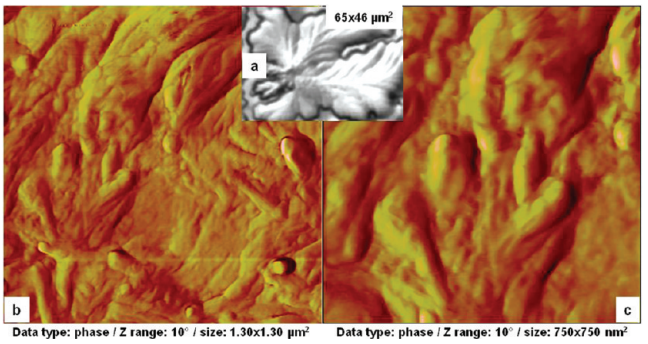

Figure 8. Tapping mode AFM images showing the submicrometer-scale structure of a dendrite (a), inside the crystallization pattern. Both images in parts b and c are characterized by cylinder-shaped domains, which reproduce at this submicrometer-scale, the finger patterns characteristic of the dendrites at the macroscopic scale.

this work opens new possibilities toward the formation and the control of self-assembly and crystallization structures of polysaccharide biopolymers, and beyond, of synthetic functional polyelectrolytes at interfaces. The emergence of the structures with guar gum whose synthesis does not involve any Na cation species, unlike SA, shows that salt traces (impurities) that may be initially contained *in the product* are neither essential nor necessary for the formation of the structures. This supports well the overall results presented throughout this work. Finally, we observed these structures for their submicrometer-scale morphology and organization, using tapping mode atomic force microscopy (AFM). These AFM observations were performed on a dendrite (Figure 8), presenting an enough smooth surface morphology to minimize experimental problems related to the strong topographical roughness intrinsic to these dendrite crystals. Although the conditions of these preliminary characterizations and the experimental problems related to the softness of the structures did not allow acceding to the nanoscale resolution of the chains organization, they already provide some insightful results regarding the structure formation. First, these AFM images (Figure 8b-c) reveal a submicrometer-scale structure characterized by nanosize (50−100 nm) cylinder-shaped domains, which reproduce in their spatial organization, the finger patterns characteristic of the dendrites at the macroscopic scale. Second, these submicrometer images clearly show that the dendrites are certainly not composed of salt crystals or other unknown contaminants, or of insoluble particles aggregates.

The next step forward in this work will focus on the fine structural characterization (AFM, diffraction) of the nanometer and molecular-scale organization of the chains inside the dendrites patterns. This might bring deeper understanding on chain conformation and packing in these *well organized self-assembly structures* and possibly the way to tune them toward the formation of desired interface crystallization patterns of polysaccharide polymers.

6. Conclusion

We have used wetting dynamics to create well-organized self-assembly and crystallization patterns of sodium alginate chains, a polysaccharide which was not known so far to crystallize spontaneously. The crystallization structures appear within the residual spot at the end of the evaporation-drying of wetting films of the aqueous solution of the polymer, prepared using ultrapure water (conductivity of 1 $\mu S \cdot cm^{-1}$), and deposited on silicon wafers. We showed that the formation of these structures can be tuned by either adjusting the concentration of the polymer, the volume of the solution, or the initial surface area covered by the wetting film at constant concentration. On the basis of the structural properties of polysaccharides, we showed that these structures are induced by the residual salt cations (Na^+) originally contained in the water, which are dragged by the receding front of the wetting film and concentrated with the polysaccharides chains within the final drying spot. The condensation of these Na^+ cations on the unbounded carboxylate anions of Na-alginate chains ultimately leads to a shortening of the Debye screening length, and an increase of chain flexibility (the persistence length decreases), driving the packing and long-range ordering of the chains (self-assembly and crystallization). Besides the insight this work brings on the behavior and structural properties of polysaccharides, it definitely shows the powerful tool that wetting dynamics constitutes for understanding, creating, and controlling structures formation at interfaces.

Acknowledgment. Dr. Haidara wishes to express special thanks to Dr. G. Chandrasekar for having so kindly helped with the centrifugation of the products. The authors are also grateful to Dr. K. Mougin for her help with AFM characterization of the structures.

Supporting Information Available: (1) Figures showing representative SEM images and corresponding EDX elemental analyses of the featureless drying area of a pure water drop on bare Si substrate, (2) figures and tables giving a representative series of full EDX characterization (elemental analysis and its spatial variation) performed across the coating, from the reference (virgin) region, toward the final drying spot, (3) a figure showing a sketch of the configuration and essential stages of the drying dynamics of the wetting film (paddle) of Na−alginate solution, (4) a movie showing the stick−slip induced thickness fluctuations, and the local dynamics at the receding front of a SA wetting film of nominal concentration, 0.25 wt %, (5) two movies showing the late stage of the evaporation-drying dynamics leading to the formation of the crystallization patterns on wetting films of SA solutions; (6) and a figure showing the experimental results illustrating the dependence of the structure formation on the concentration of the SA solution. This material is available free of charge via the Internet at http://pubs.acs.org.

References and Notes

(1) Baffoun, A.; Haidara., H.; Dupuis, D.; Viallier, P. *Langmuir* **2007**, *23*, 9447–9454.
(2) Baffoun, A.; Viallier, P.; Dupuis, D.; Haidara, H. *Carbohydr. Polym.* **2005**, *61*, 103–110.
(3) Haidara, H.; Baffoun, A.; Viallier, P. *Polymer* **2004**, *45*, 833–8338.
(4) Pu, G.; Guo, J.; Gwin, L. E.; Severtson, S. J. *Langmuir* **2007**, *23*, 12142–12146.
(5) Gonuguntla, M.; Sharma, A. *Langmuir* **2004**, *20*, 3456–3463.
(6) Fabia, J.; Ślusarczyk, Cz.; Gawlowski, A. *Fibres Text. East. Eur.* **2005**, *13* (January/December), 114−117.
(7) Atkins, E. D. T. *Pure Appl. Chem.* **1977**, *49*, 1135–1149.
(8) Li, L.; Fang., Y.; Vreeker, R.; Appelqvist, I. *Biomacromolecules* **2007**, *8*, 464–468.
(9) Borchard, W.; Kenning, A.; Kapp, A.; Mayer, C. *Int. J. Biol. Macromol.* **2005**, *35*, 247–256.
(10) Simeone, M.; Alfani, A.; Guido, S. *Food Hydrocolloids* **2004**, *18*, 463–470.
(11) Shchipunov, Y. A.; Postnova, I. V. *Polym. Sci. Ser. A* **2006**, *48*, 171–176.
(12) Peng, P.; Voelcker, N. H.; Kumar, S.; Griesser, H. J. *Biointerphases* **2007**, *2*, 95–104.
(13) Finotelli, P. V.; Morales, M. A.; Rocha-Leao, M. H.; Baggio-Saitovitch, E. M.; Rossi, A. M. *Mater. Sci. Eng., C* **2004**, *24*, 625–629.
(14) El-Molla, M. M.; El-Sayad, H. S. *Adv. Polym. Technol.* **2001**, *20*, 58–71.
(15) Schneider, R.; Sostar-Turk, S. *Dyes Pigments* **2003**, *57*, 7–14.
(16) Nie, H.; He, A.; Zheng, J.; Xu, S.; Li, J.; Han, C. C. *Biomacromolecules* **2008**, *9*, 1362–1365.

(17) It is worth noting in this respect that if one assumes the total drainage of the salt traces initially contained in the water, the evaporation of a pure drop of 100 μL of the Milli-Q water of 1 μS/cm on the bare Si substrate would lead, in the tiny residual micronsize spot of $\sim 10^5$ μm^3, to a salt concentration as high as 10^2-10^3 g/L.
(18) Basu, S.; Nandakumar, K.; Masliyah, J. H. *J. Colloid Interface Sci.* **1997**, *190*, 253–257.
(19) Redon, C.; Brochard-Wyart, F.; Rondelez, F. *Phys. Rev. Lett.* **1991**, *66*, 715–718.
(20) Carré, A.; Eustache, F. *Langmuir* **2000**, *16*, 2936–2941.
(21) Deegan, R. D.; Bakajin, O.; Dupont, T. F.; Huber, G.; Nagel, S. R.; Witten, T. A. *Nature* **1997**, *389*, 827–829.
(22) Mougin, K.; Haidara, H. *Langmuir* **2002**, *18*, 9566–9569.
(23) Hoffman, J. D.; Miller, L. R. *Polymer* **1997**, *38*, 3151–3212.
(24) Anit, E.; Cyriac, J.; Ittyachen, M. A. *Bull. Mater. Sci.* **2001**, *24*, 431–434.
(25) Wang, Z-YS.; Zhang, Q.-Z.; Konno, M.; Saito, S. *J. Phys. II Fr.* **1993**, *3*, 1–7.
(26) Zeng, H.; Jiang, K.; Zhang, Q.; Wang, J. *Chem. Phys.* **1996**, *211*, 507–513.
(27) Zhang, H.; Wang, H.; Wang, J.; Guo, R.; Zhang, Q. *Polym. Adv. Technol.* **2001**, *12*, 740–74.
(28) Dobrynin, A. V.; Colby, R. H.; Rubinstein, M. *Macromolecules* **1995**, *28*, 1859–1871.
(29) Ohki, S.; Ohshima, H. *Colloids Surf. B: Biointerfaces* **1999**, *14*, 27–45.
(30) Gittings, M. R.; Cipelletti, L.; Trappe, V.; Weitz, D. A.; In, M.; Lal, J. *J. Phys. Chem. A* **2001**, *105*, 9310–9315.
(31) Ma, X.; Pawlik, M. *Carbohydr. Polym.* **2007**, *70*, 15–24.